Scientific Research Publishing

Spectroscopic Characterization of the Interaction between Dopamine and Human Serum Albumin

Imtiaz M. Khalid[1], Sawsan E. Abu Sharkh[2], Husain Samamarh[2], Rania Alfaqeeh[2], Musa M. Abuteir[2], Saqer M. Darwish[2]

[1]Department of Chemistry, Birzeit University, Birzeit, Palestine
[2]Department of Physics, Al Quds University, Beit Hanina, Abu Dis, al-Bireh, Palestine
Email: imtiazkhld@yahoo.com

Abstract

The interactions of HSA with DA have received great attention nowadays due to its significant effect in the biomedical field and overall health. The main aim of this work is to examine the interaction between DA and HSA at physiological conditions. Upon addition of DA to HSA, the fluorescence emission was quenched with quenching constant $K_q = 1.32 \times 10^9$ L·mol^{-1}·s^{-1} and the binding constant of DA with HSA is found to be K = 4.4×10^2 mainly indicating dynamic quenching. The HSA conformation was altered upon binding of DA to HSA with an increase in α-helix and a decrease in β-sheets suggesting unfolding of HSA secondary structure due to weak intermolecular interaction with HSA. In view of the evidence presented, it is important to understand the details of the interactions of HSA with DA which will be crucial in the design of new DA-inspired drugs and help revealing vital details to better understand the HSA's role as a transporter for many drugs.

Keywords

Dopamine, HSA, Binding Constant, Non-Linear Stern-Volmer Plot, Protein Secondary Structure, FT-IR Spectroscopy

1. Introduction

Dopamine (DA), chemical structure provided in the top part of **Figure 1** [1], is a catecholamine neurotransmitter synthesized within the brain in the dopaminergic neurons and is involved in regulating multiple functions including movement and memory. DA transmits signals between neurons throughout human
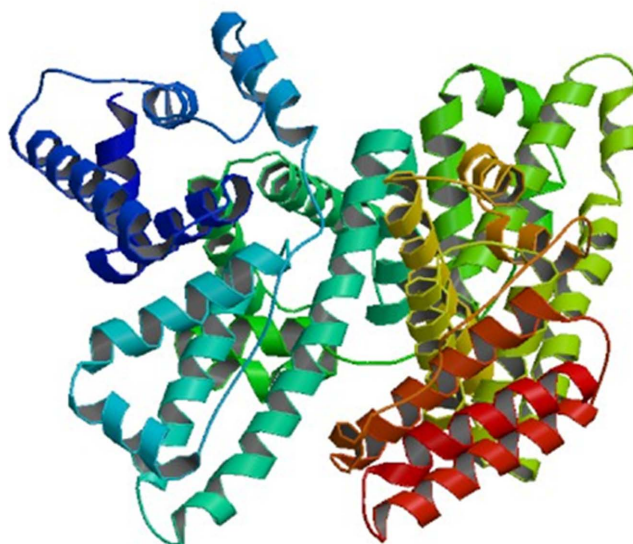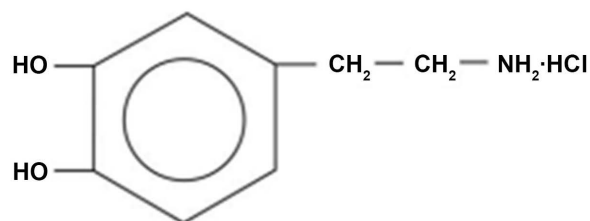
Figure 1. Chemical structure of dopamine hydrochloride (top). Secondary structure of HSA (bottom).

brain and body. The elevated or reduced dopamine level may cause memory loss related diseases, attention deficit, hyperactivity disorder, daydreaming and not being able to stay on task. Any changes in the levels of this vital neurotransmitter chemical have been proven to be related to several dopaminergic neurological diseases depending on the affected region in the brain [2] [3] [4] [5]. For example, neurocognitive disorders related to memory, attention, and problem-solving functions result from decline of DA in frontal lobes of the brain which controls the flow of information from other areas of the brain [6] [7] [8]. Therefore, DA is considered a major target for drug designing applied in the treatment of neurological diseases.

Inadequate DA levels due to the loss of DA-producing cells have been related Parkinson's disease which is associated with a loss in the ability of well controlled movements [9] [10] [11]. Despite the ongoing research to understand these devastating disorders, the sophisticated causes of dopaminergic cells' loss in Parkinson's disease are only partially understood.

1.1. Human Serum Albumin (HSA)

Human serum albumin (HSA), secondary structure provided in the bottom part

of Figure 1 [12], is the most prominent protein in the human blood plasma and it constitutes about 60% of the total plasma proteins. It is a single-chain polypeptide consisting of 585 amino acids residues stabilized by 17 disulfide bridges and has a molecular mass of 66.5 kDa. HSA high importance is due to its many important physiological functions [13] [14]. HSA is made up of three similar structural domains I, II, and III. Each domain is further divided into subdomain A and B. It is well documented that subdomains IIA and IIIA are known as the major drug binding sites for the majority of heterocyclic and aromatic compounds [12] [13]. Recent investigation has demonstrated the capacity of subdomain IB in binding drugs making it a potential for various drugs delivery [15]. These binding sites empower the HSA with an exceptional ability in binding various ligands, which adds to its biological importance in delivering number of drugs in the blood system to their targeting organs/tissues within the human body [16] [17]. Generally, HSA binds reversibly with wide range of drugs however some drugs with high affinity for HSA limit the drug distribution—of free form and the bound form—as well as the elimination of the drugs. In addition, the HAS-drug interactions play an important role in understanding the efficiency of the drug as determined by the free fraction of the drug [18] [19].

1.2. Alzheimer's Disease (AD)

AD, affecting millions of individuals worldwide, is an irreversible neurodegenerative disorder characterized by progressive cognitive decline and dementia [20]. The decline in cognitive function affects recent memory first then slowly spreads to other regions of the brain. As of now, the exact cause of AD is not known and currently there is no cure for this devastating disease. Therefore, any available treatment is meant to slow the progression of AD and relieves its symptoms. It has been suggested and well documented that AD originates in the brain [21] but a recent investigation have indicated that AD could have been triggered by breakdowns elsewhere in the body. This finding makes is promising in preventing AD from reaching the brain if proper drug targets the toxin protein and removes it while in the blood without the need to act directly on the brain, which is a very challenging task to accomplish and hard-to-reach target safely [22] [23]. In addition, electrical signaling responsible for learning and memory is usually diminished in people with AD [24].

1.3. Parkinson's Disease (PD)

PD, a neurological disorder that affects movement control, neurons progressively degenerate and as a result, the amount of DA available for neurotransmission in the brain is lowered [25] [26]. The main symptoms of PD due to DA imbalance include resting tremor, rigidity, a gradual slowness of natural movement, poor balance and diminished motor coordination [9] [27].

The underlying cause of PD is the progressive loss of dopaminergic neurons in some neurons and the presence of Lewy bodies—abnormal protein aggregates—in the remaining neurons [24]. The neural loss leads to dopamine defi-

ciency which is believed to be responsible neurodegenerative "motor disease". The main therapy to treat PD is by dopamine replacement merely relieves the associated symptoms but the disease continues its progression. Therefore, there is a need for understanding the process of the neurological degeneration to develop effective drugs to stop the degeneration [10] [11].

In addition to PD, alterations in the dopamine levels have been consistently observed and reported in AD patients, including lower levels of dopamine (DA) [28] [29]. Although research investigations have resulted in developing few theories about AD, until now there is no definite reason standing out as the cause of this disturbing disease [21] [30] [31]. There is evidence supporting the conception that dopaminergic system dysfunction has a role in cognitive decline symptoms of AD, however, the cause of dopaminergic system dysfunction in AD remains to be elucidated [2] [24] [32].

Drug binding to HSA plays a major role in the drug efficacy—the ability of a drug to provide a beneficial effect—which is affected by drug distribution—the process of delivering a drug from the plasma to the tissue(s) where the drug's actions are needed. Most of the drugs used by humans are bound to HSA which influences the drug distribution, absorption and efficiency [15] [16] [17] [18] [19] [33] [34] [35]. Since dopamine is recognized for its high pharmaceutical value as a potential candidate for treatment of neurological disorders such as AD and PD [8] [36] and it's binding to HSA is not quite understood, therefore, the interaction of dopamine, a potential drug, with HSA is highly important to better understand the drug-protein complex in terms of structural changes and stability to better elucidate its pharmacological importance. Therefore, the interaction of dopamine and HSA is crucial to better understand the HSA-DA complexation, provide significant information about HSA-DA stability as a complex, and underline the role of HSA in delivering DA to the blood stream. Similar to previous investigations with various other drugs [37] [38], this endeavor is fueled by spectroscopic characterization to investigate the interaction between the HSA and DA and determine the complex stability associated with this binding. To reach this, we used fluorescence in combination with UV absorption spectroscopy and Fourier transform infrared (FTIR) spectroscopy to study the interaction of DA with HSA to characterize the effect of this drug on HSA conformational changes resulting from such complex. FTIR spectroscopy is reliable in monitoring conformational changes when proteins interact with drugs due to detection of functional groups' changes due to interactions between the drug and the HSA thus affecting the overall secondary structure of the protein. Similar to other chemical compound, proteins have amide groups with the general structure of (—C(=O)−N—) which are clearly detected by FTIR. Therefore, any changes resulting from stabilization effects due to intermolecular forces, will cause changes to vibrational modes of the amide groups of the proteins. Similarly, fluorescence spectroscopy is a powerful analytical chemistry technique in providing structural changes information due to quenching upon intermolecular

forces. Thus, fluorescence contributes in providing data to calculate binding constants and binding sites.

2. Experimental

2.1. Samples' Preparations and Materials

HSA protein (66,500 Da) and dopamine (189.2 g/mol) in powder form were purchased from Sigma Aldrich chemical company and were used without any further purifications. HSA stock solution was prepared in a concentration of 80 mg/ml dissolved in phosphate buffered saline with pH of 7.4 which corresponds to 1.2 mM. The final concentration of HSA in the HSA-DA complex was 40 mg/ml equivalent to molarity of 0.6 mM which is comparable to its concentration in the blood [15].

Dopamine stock solution with molarity of 4.8 mM, was prepared by dissolving dopamine hydrochloride in enough distilled water to prepare DA stock solution.

DA standard solutions were prepared by successive dilutions. The HSA-DA complexes were prepared by mixing equal volumes of 1.2 mM HSA molarity and each of the standard DA solutions. The final concentration of HSA was kept at (40 mg/ml) in all samples while the concentrations of dopamine in the final HSA dopamine solutions was reduced to be as (0.15 mM, 0.3 mM, 0.4 mM, 0.5 mM, 0.6 mM, 1.0 mM, 1.2 mM and 2.4 mM).

2.2. Thin Film Preparation

Silicon windows (NICODOM Ltd.) were used as spectroscopic cell window. 60 µl of each sample of HSA-DA was spread on silicon window using spincoater to obtain equal thickness of each sample, then incubator was used to evaporate the solvent to obtain transparent thin film on the silicon window. All solutions were prepared at the same time at room temperature and were stored under the same conditions.

3. Instrumentation

3.1. FT-IR Spectroscopic Measurements

The FT-IR measurements were obtained used Bruker IFS 66/S spectrophotometer equipped with a liquid nitrogen-cooled MCT detector and KBr beam splitter. Silicon windows (NICODOM Ltd) were used as spectroscopic cell windows. Complexes' solutions (0.15, 0.3, 0.6, 0.7, 0.9) mM were prepared at room temperature. 60 µL of each sample of HSA-DA was spread on silicon window using spin coater to obtain equal thickness of each sample, and then was incubated for two hours to evaporate the solvent in order to obtain transparent thin film on the silicon window. The spectrophotometer was continuously purged with dry air during the measurements. The absorption spectra were obtained in the range of (400 - 4000) cm^{-1}. A spectrum was taken as an average of 60 scans to enhance the signal to noise ratio, and the spectral resolution was at 4 cm^{-1}. The aperture used in this study was 8 mm, since it gave the best signal to noise ratio. Baseline

correction, normalization and peak areas calculations were performed for all the spectra by OPUS software. The peak positions were determined using the second derivative of the spectra. The infrared spectra of HSA and the HSA-DA complexes were obtained in the region of (1200 - 1700) cm^{-1}. The FTIR spectrum of free HSA was acquired by subtracting the absorption spectrum of the buffer solution from the spectrum of the protein solution. For the net interaction effect, the difference spectra {(HSA-DA) - (HSA)} were generated using the featureless region of the spectra at (1800 - 2200) cm^{-1}.

3.2. UV-VIS Absorption Spectra

The data was collected using 5 µL samples using NanoDrop ND-1000 Spectrophotometer for the free HSA (40 mg/ml or 0.6 mM) and for the HSA-DA complexes solutions with the following concentrations (0.15, 0.3, 0.4, 0.5, 0.6, 1.0, 1.2, and 2.4) mM. UV measurements were repeated for all the samples and no significant differences were observed. The UV-absorption spectra of HSA-DA complex are obtained at the wavelength of 280 nm.

3.3. Fluorescence

The fluorescence measurements were obtained using NanoDrop ND-3300 Fluorospectometer for the following complexes concentration (0.15, 0.3, 0.4, 0.5, 0.6, 1.0, 1.2, and 2.4) mM at 25°C. The excitation source comes from one of three solid-state light emitting diodes (LEDs) including UV LED with maximum excitation 365 nm, Blue LED with excitation 470 nm, and white LED from 500 to 650 nm excitation. A 2048-element CCD array detector covering 400 - 750 nm, is connected by an optical fibre to the optical measurement surface. The excitation is done at the wavelength of 360 nm and the maximum emission wavelength is at 440 nm.

4. Results

4.1. UV-Absorption Spectroscopy

The UV absorbance spectra of different concentration of dopamine with a fixed concentration of HSA which were scanned over a range of 220 - 350 nm are presented in Figure 2. Each spectrum indicates two absorption maximum wavelengths at about 230 and 280 nm. The figure shows direct relationship between the increase in peak intensity of the HSA-DA complex and the concentration of the DA. This increase in intensity is due to interaction between HSA and DA as monitored in buffered solution by scanning the wavelengths. As indicated in the figure, there is a clear absorption signal for free DA.

The reciprocal plot of $1/(A - A_o)$ versus $(1/l)$ is linear as indicated in Figure 3. When a fixed concentration of *HSA* was allowed to complex with various amounts of *DA*, there is a linear increase in the UV absorbance of *HSA*. A binding constant for the HSA-DA complex was calculated using UV spectra according to published methods [16] with the assumption that there is one-to-one
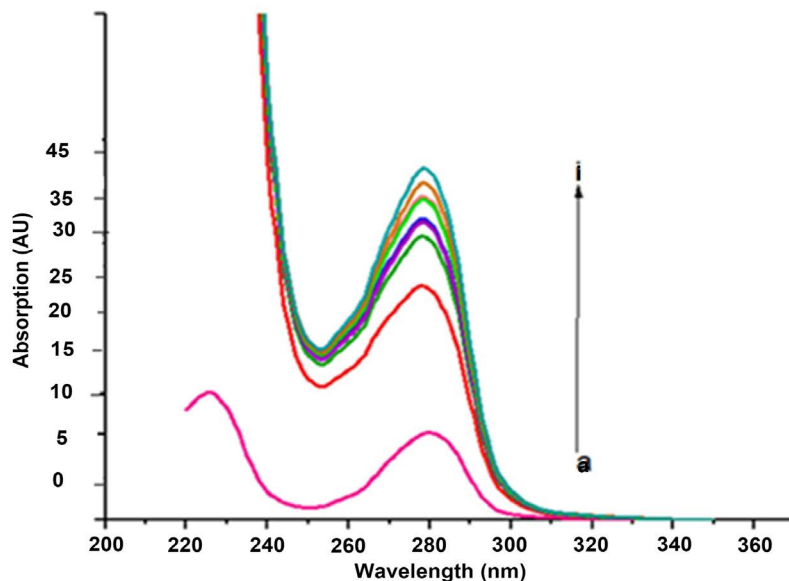
Figure 2. UV absorbance spectra of HSA-DA in 0.1 M PBS with pH 7.4 at 25˚C. Free HSA (40 mg/mL, 0.6 mM) and free HSA with different DA concentrations (a = free DA (4.8 mM), b = free HSA (0.6 mM), c-i correspond to HSA-DA complexes with (0. 3, 0.4, 0.5, 0.6, 1.0, 1.2 and 2.4) mM DA respectively.
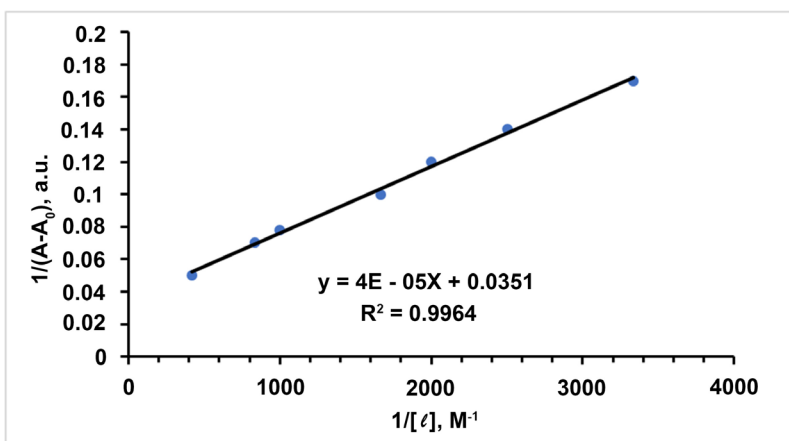

Figure 3. The plot of $1/(A-A_0)$ vs. $1/l$ for free HSA (40 mg/mL, 0.6 mM) and with different HSA-DA complex concentrations in 0.1 M PBS with pH 7.4.

interaction between *HSA* and *DA* in aqueous solution to establish chemical equilibrium as in the following equation.

$$HSA + DA \leftrightarrow HSA : DA \tag{1}$$

The corresponding formation/binding constant:

$$K = [HSA : DA]/[DA][HSA] \tag{2}$$

on the following equation.

$$1/(A - A_0) = 1/(A - A_0) + 1/k(A_\infty - A_0) * 1/l \tag{3}$$

where A_o corresponds to the initial absorption of *HSA* at 280 nm in the absence of *DA*, A_∞ is the final absorption of the *HSA*, and *A* is the recorded absorption at

different *DA* concentration (*I*).

The binding constant (*K*) for HSA-DA complex was estimated from the ratio of the intercept to the slope and was found to be 8.54×10^2 M^{-1}. The value for the binding constant is an indication of a weak intermolecular force interaction between the HSA and DA when compared to reported HSA-drug interaction with binding constant in the range of 10^4 and 10^6 M^{-1} [39] The importance of the binding constant value stems from its valuable application in drug delivery and pharmacokinetics [17] therefore, absorbance measurements were constantly repeated and similar results were obtained consistently. In addition, absorbance spectra were recorded for DA free with various concentrations corresponding to those of DA concentrations in the final HSA-DA complex. To further investigate the nature of the complexation-interaction, the absorbance value from the spectra of free HSA was added to the absorbance value of the free HSA at 280 nm. The corresponding added absorbances' values clearly indicate that the signal obtained for the various individual added concentrations of the free HSA and free DA are comparable in magnitude to those of HSA-DA complex with same final concentration. This result supports the speculation that the interaction between HSA and DA is weak interaction.

4.2. Fluorescence Emission Spectroscopy

The emission spectra in the range of 400 to 750 nm were obtained for HSA-DA spectra are shown in Figure 4. When a fixed concentration of HSA is titrated with various amounts of DA, a decrease in the fluorescence emission of HSA is clearly presented. The quenching took place in a concentration dependent manner; an increase in DA concentration led to decrease in HSA fluorescence intensity. It is well established that HSA fluorescence is mainly due to Tryptophan (Trp), which is located at 214 position of subdomain IIA with very minor contribution from tyrosine (Try) and phenylalanine which provide very low quantum yields and therefore can be ignored [19] As a result, the fluorescence quenching is caused by addition of different concentrations of DA which causes quenching of fluorescence emission. This quenching could be a result of DA binding to HSA – a major drug carrier protein in the human blood plasma. Another reason is the possibility of formation of HSA-DA complex. There is no noticeable peak positional shift indicating that no major structural alternations of HSA upon binding with DA. Peak shifts, appearance of new peaks, disappearance of existing peaks or various combinations of the mentioned are main characteristic of major structural changes.

The HSA fluorescence is decreased upon increasing concentrations of DA, which indicates that the DA is interacting with HSA in the surrounding of the HSA main fluorescent residue Trp214 in subdomain IIA. The interaction between the DA and HSA can affect HSA fluorescence upon binding to DA due to the quenching ability of a tryptophan residue upon colliding with DA. Careful examination of the absorption spectra does not show and major changes and
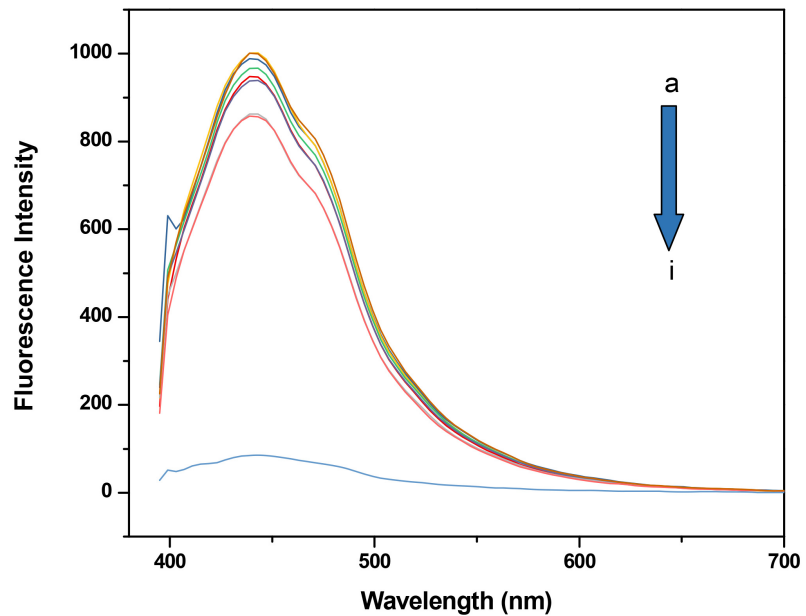
Figure 4. Fluorescence emission spectra of free HSA and HSA-DA in 0.1 M PBS with pH 7.4, λex = 360 nm, λem = 439 and temperature at 25˚C. a = Free HSA (40 mg/mL, 0.6 mM), *i* = free DA (4.8 mM), and (b-h) correspond to HSA with different DA concentrations (b = 0. 3, 0.4, 0.5, 0.6, 1.0, 1.2, and 2.4) mM DA.

very little changes is observed on the absorption spectra of the HSA shape as the DA concentration is added which is an indication of minor conformational changes due to collisional quenching [40].

Further, to elucidate the nature of the quenching mechanism as static or dynamic in the HSA-DA system, Stern-Volmer equation [35] is used to plot F_0/F versus l and the result is shown in **Figure 5**. The Stern-Volmer plot is non-linear, indicating that both types of static and dynamic quenching occur. HSA is quenched both by collisions and by complex formation with DA. Hence,

$$F_0/F = \left(1 + K_{sv}[DA]\right) * \left(1 + K_D[DA]\right) \tag{4}$$

where F and F_0 are the fluorescence intensities with and without quencher, K_D is the dynamic quenching constant of the biomolecule and K_{sv} is the Stern-Volmer quenching constant due to static quenching. This modified second order form of the Stern-Volmer equation with respect to DA concentration, accounts for the both static and dynamic quenching occur for the same fluorophore. When quenching is due to static quenching, the second parenthesis in Equation (4) is ignored and when the quenching is dynamic the first parenthesis is ignored. However, when both static and dynamic quenching are present, one must account for each type.

Fluorescence quenching can be induced by different mechanisms, which are usually classified into dynamic and static quenching. Dynamic quenching arises from collisional encounters between the fluorophore and quencher, and static quenching resulting from the formation of a ground state complex between the fluorophore and the quencher [40].
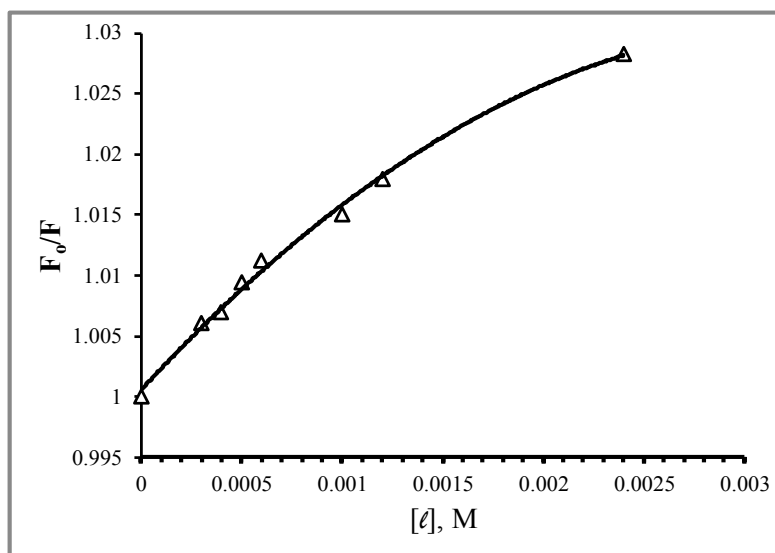
Figure 5. The Stern-Volmer plot for HSA-DA complexes.

To further understand the nature of quenching, the quadratic equation was solved using Excel for the K_D and K_{SV} values which were found to be $K_D = K_{SV} = 6.60 \text{ M}^{-1}$.

Using calculated K_D value of 6.6 M^{-1} and τ_0 as 5×10^{-9} s for HSA [40] which is typical for diffusion controlled reaction, the quenching constant, k_q, is calculated from the $k_{sv} = k_q \tau_0$ relation according to Stern-Volmer equation and which is determined to 1.32×10^9 L·mol^{-1}·s^{-1} which is about the same as for collisional dynamic quenching constant for various quenchers with biopolymer (maximum value of 2×10^{10} L·mol^{-1}·s^{-1}) [12] [13]. This result implies that quenching is mainly due to dynamic collision and not to complex formation, but rather a dynamic quenching is mainly dominated [40] [41].

4.3. Accessibility of Tryptophan in HSA to Quenching by DA Using Fluorescence

When dynamic collisional quenching dominates as quenching type of fluorescence for HSA with drugs, it usually results in deviation from linearity of Stern-Volmer plots. Therefore, it becomes necessary to further analyze the non-linear Stern-Volmer plots to determine if the quenching is purely collisional and to determine the accessibility fluorophores. Hence the following modified Stern-Volmer can be used: [40].

$$F_0/F = \left(1/f_a K_a\right) * \left(1/[DA]\right) + \left(1/f_a\right) \tag{5}$$

where ΔF is the difference between the unquenched fluorescence and the quenched fluorescence, f_a is the fraction of the initial fluorescence that is accessible to quencher, K_a is the Stern-Volmer quenching constant of the accessible fraction, and $[DA]$ is the dopamine concentration. The K_a can be calculated from the slope of the straight-line equation resulting from plotting $F_0/(\Delta F)$ vs. $1/[DA]$ as shown in **Figure 6**. The obtained value of effective binding constant,
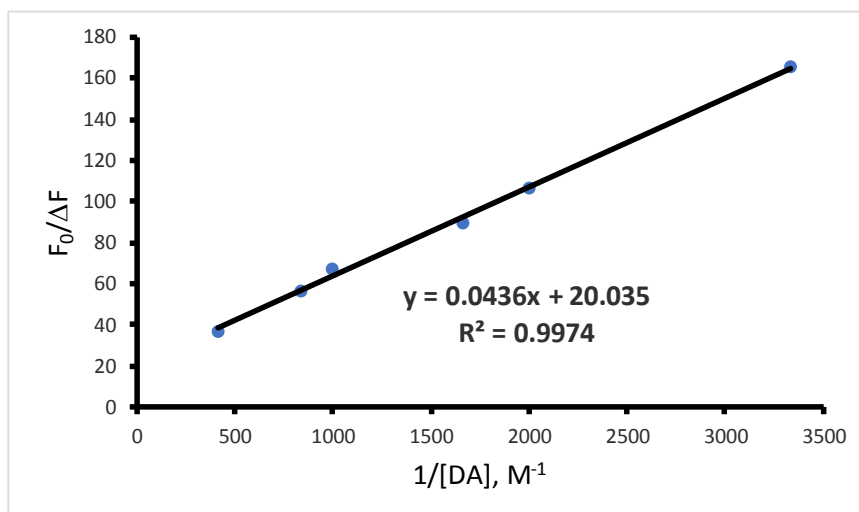
Figure 6. Modified Stern-Volmer plot for HSA-DA complexes for accessibility determination.

K_a is determined to be determined to be 4.4×102 M^{-1} and the accessible fraction $f_a = 0.05$ indicating that the Trp214 is not accessible for biding with DA which is in agreement with the small effective binding constant.

4.4. FT-IR Spectroscopy

FT-IR is used widely to analyze IR bands of structural characterization of proteins and provide clear information of any changes might occur due to various changes leading to decrease/increase in intensities of the original peaks as well as any shifts (blue/red due to interaction and or structural changes). HSA shows number of amide bands due to vibrations of various peptides within the protein. [42] Specifically, the amide groups of the peptides represent characteristic vibrational modes (amide modes) which are sensitive to protein structures and any incurred changes might cause structural changes. IR spectral data for the HSA give rise to nine characteristic IR absorption bands, namely, amide A, B, and I-VII [43] [44] [45].

Amide I band ranges from 1700 to 1600 cm^{-1} and is mainly due to C=O stretching vibrations of the peptide linkages. Amide II in the range of 1600 - 1480 cm^{-1} is due to the coupling of the N—H in-plane bending to C—N stretching vibration, while amide III band ranging from 1330 to 1220 cm^{-1} is due to the C—N stretching mode coupled to the in-plane N—H bending mode [45].

The FT-IR absorption spectra in the region of (1800 - 1200) cm^{-1} are shown in **Figure 7** for HSA and various HSA-DA complexes while HSA second derivatives are shown in **Figure 7** for free HSA (bottom) and HSA-DA complexes (top) while the difference spectra corresponding to free HSA and HSA-DA complex with various DA concentrations are shown in **Figure 8**. In addition, band assignments for the same spectra are presented in **Table 1** according to region and DA concentrations. The second derivative of free HSA is shown in
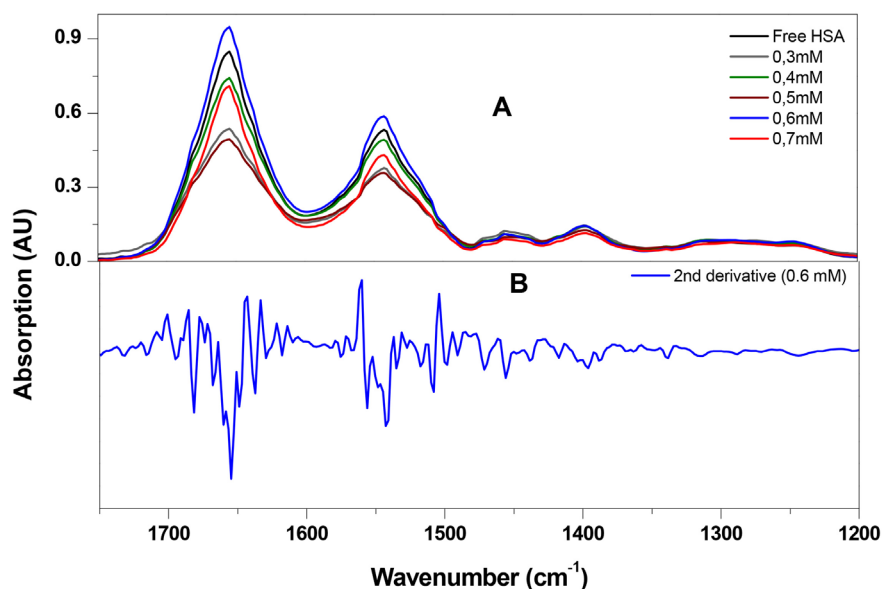
Figure 7. The FT-IR spectrum of 0.6 mM HSA free (bottom) and the spectra (second derivative) of DA-HSA complex (top) (a-f). DA concentration of 0.0 mM, 0.3 mM, 0.4 mM, 0.5 mM, 0.6 mM and 0.7 mM.

Figure 8. FT-IR spectra (top two curves, a (HSA free) and b (HSA + 0.7 mM DA) and differences spectra of HSA free and various DA-HSA complexes (c, d, e, f and g) with concentration of (0.3 mM, 0.4 mM, 0.5 mM, 0.6 mM and 0.7 mM).

Figure 8 (bottom) where the spectra is dominated by absorbance bands of amide I and amide II at 1655 cm^{-1} 1540 cm^{-1} respectively. It is clear from the figure that as the DA concentration increases, the intensity of the 1655 cm^{-1} 1540 cm^{-1} peaks decrease.

For DA-HSA interaction, the amide bands of HSA infrared spectra over all

Table 1. absorption peak assignment (in wavenumbers, cm^{-1}) for HSA-DA at different concentration.

Bands	Range (cm^{-1})	Free HSA	DA concentrations				
Amide I	1700 - 1600	0.0	0.3 mM	0.4 mM	0.5 mM	0.6 mM	0.7 mM
	β-sheets	1609	---	1609	---	1610	1610
	β-sheets	1622	1621	1622	1622	1623	1623
	Random	1636	1636	1636	1636	1636	1636
	α-helix	1656	1654	1655	1655	1655	1655
	Turns	1681	1681	1681	1680	1680	1681
	β-sheets	1695	1695	1695	1695	1695	1695
Amide II	1600 - 1480						
	β-sheets	1493	1494	1494	1495	1495	1494
	Random	1520	1523	1521	1523	---	---
	α-helix	1540	1542	1543	1543	1544	1544
	Turn	1574	1575	1576	1576	1575	1575
	β-sheets	1592	1594	1593	1593	1593	1593
Amide III	1320 - 1220						
	β-sheets	1231	1231	1231	1231	1231	1231
	β-sheets	1245	1245	1245	1245	1245	1245
	Random	1268	1271	1268	1267	1270	1268
	turn	1294	1293	1293	1293	1291	1290
	α-helix	1310	1309	1310	1310	1310	1310

shift is listed clearly in Table 1. In amide I band, the peak positions have shifted from the HSA free to HSA-DA after addition of 0.7 mM DA as follows: 1622 → 1623 cm^{-1}, 1656 → 1654 cm^{-1}, 1681 → 1680 cm^{-1}. In addition, the peak at 1609 cm^{-1} was fluctuating disappearing and appearing at various concentrations as shown in the table. For amide II, the peak positions have shifted as follow: 1493 → 1494 cm^{-1}, 1520 → 1523 cm^{-1} and disappeared at the last two highest DA concentration, 1540→ 1544 cm^{-1}, 1574 → 1575 cm^{-1} and 1592 → 1593 cm^{-1}. In amide III region, the only peak shift is on: 1294 → 1290 cm^{-1}.

The 1656 cm^{-1} and 1540 cm^{-1}, which correspond to amide I and amide II, respectively represent the location of both the amide bonds orientation are sensitive to the HSA secondary structure because both groups of C=O and the N-H bonds are involved in the hydrogen bonding that takes place between the different elements of secondary structure [17] [46]. The overall change in peaks positions indicate HSA secondary structural changes due to interaction with DA. This shift in peak positions is mainly contributed to collisional electrostatic interaction between the HSA and the DA. Shifts to lower wavenumbers for the major peak in amide I *i.e.* 1656 → 1654 cm^{-1} is mainly due to stabilization by intermolecular interaction between the non-bonding pair of electrons on the oxy-

gen of the carbonyl C=O and the hydrogen of N—H thus causing the corresponding amide II shift from 1540 to 1544 cm^{-1}. Looking at the overall data in Table 1, it is obvious that the peak change (appearance, disappearance or shift) was stabilized or reached a steady behavior when the ratio of DA to HSA was approaching 1, specifically when the DA concentration reached 0.6 mM which corresponds to 1:1 ratio with the HSA and beyond.

FT-IR spectra for the HSA-DA interaction are shown in Figure 8. The FT-IR spectra (top two curves) and difference spectra {HSA-DA complex—HSA free} for HSA-DA different ratios complexes in amide I and amide II regions are clearly presented. There is no appearance of any new peaks or major shift in peak position. However, in amide I region, there is a negative peak at 1655 cm^{-1} with little shift of position that increases in intensity as the DA concentration is increased which corresponds to increase in HSA-DA complex concentration. Similar behavior is noted in amide II region with a negative feature at 1542 cm^{-1}. The negative peaks behavior is attributed to the change in intensity of amide I and II bands which is a result of change of the secondary structure of HSA after combination with DA due to intermolecular interaction between the DA and the C=O and or N—H groups [46] [47].

The component bands of three amide regions, I, II and III were attributed according to the well-established principle [48] [49] as follows: the bands in the range of 1610 - 1640 cm^{-1} are generally assigned to -sheet, bands in the range 1640 - 1650 cm^{-1} correspond to random coil, bands in the range 1650 - 1658 cm^{-1} are attributed to α-helix and the 1660 - 1700 cm^{-1} bands correspond to β-turn structure. The absorption bands in amide II consist of four components assigned in the following order: 1488 - 1500 cm^{-1} to β-sheets, 1504 - 1525 cm^{-1} to random coil, 1527 - 1560 cm^{-1} to α-helix and 1564 - 1585 cm^{-1} to turn structure. The component bands of amide III have been assigned as follows: 1330 - 1290 cm^{-1} to α-helix, 1290 - 1270 cm^{-1} to β-turn and 1220 - 1250 cm^{-1} to β-sheets. Percentage determination of the contribution of each secondary structural element in the HSA-DA complex secondary structure was carried out based on the assignment criterion for each of the HSA free and after the interaction with DA in amides I, II, and III. The quantitative analysis of the HSA was performed to determine any change in the secondary structure of HSA due to complexation with DA.

The components bands of amide I, II, and III regions were assigned using Fourier self-deconvolution (FSD) and second derivative resolution with curve fitting as shown in Figure 9.

For amide I band, the components are assigned as follows: 1606 - 1620 cm^{-1} represent β-sheet, 1620 - 1647 cm^{-1} represent random coil, 1649 to 1670 cm^{-1} correspond to α-helix, 1672 - 1687 cm^{-1} to turn structure and 1687 - 1700 cm^{-1} correspond to β-antiparallel. For amide II region, the absorption bands are assigned in the following order: 1487-1506 cm^{-1} to β-sheet, 1506 - 1523 cm^{-1} to random coil, 1523 - 1558 cm^{-1} to α-helix, 1560 - 1585 cm^{-1} to turn structure and 1585 - 1600 cm^{-1} to β-antiparallel. For amide III region, the bands are assigned
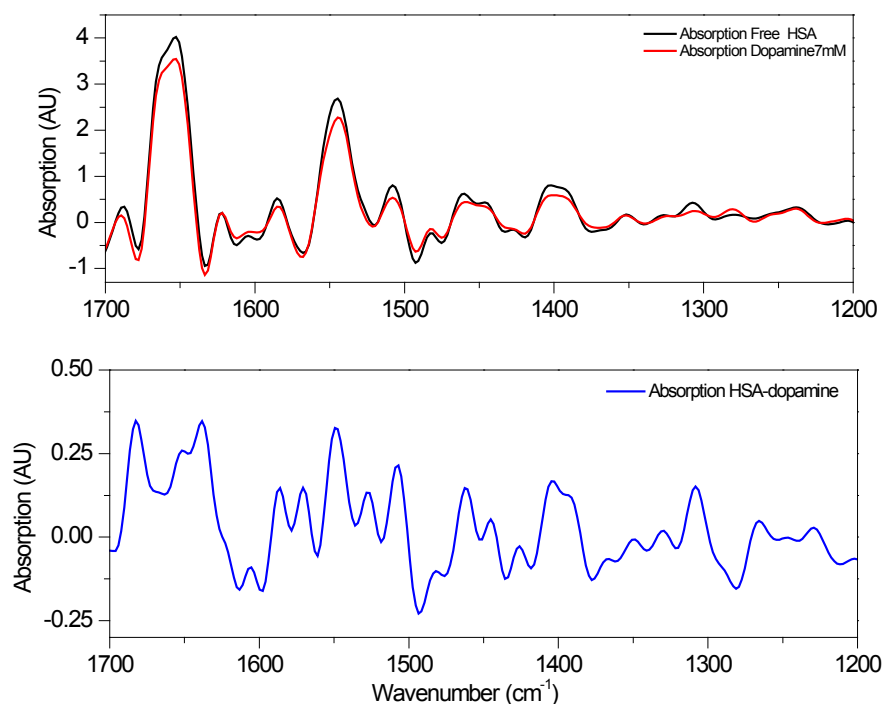
Figure 9. Fourier self-deconvolutions (FSD) spectra subtraction: top {free HSA - HSA-DA (0.7 mM)}, bottom the final result of the subtraction.

as follows: 1220 - 1256 cm^{-1} to β-sheet, 1259 - 1287 cm^{-1} to random coil, 1288 - 1302 cm^{-1} to turn structure, and 1302 - 1331 cm^{-1} to α-helix. Most investigations have revealed that amid I bands are most sensitive in contributing to the secondary structure change however many studies reported informational contribution from amide II and III and can be used to study the secondary structure of protein. [50] [51] [52].

In this work, the percentage of each secondary element of HSA secondary structure were calculated using normalization to integrate areas of the components bands in amide I, II, and III divided by the total area. The obtained values represent relative intensities for each of the secondary element with the specified region while the area under each secondary element corresponds to its percentage. **Figure 10** shows the percentages determination for the secondary structure of HSA in amide I region. Similar figures were obtained for each of amide II and amide III regions. The obtained data in **Table 2** is extracted from **Figure 10** and curve-fitted for amide I, II and III regions and secondary structure determinations of the HSA free and its DA various complexes in dehydrated films. The table clearly lists the percentages of each secondary structure of HSA before and after the interaction with DA at different concentration. As a general trend, as DA concentrations are increased, *α*-helix percentage increased in the three amide regions which is accompanied by overall decrease *β*-sheet percentages in the same regions.

The increase in *α*-helix percentage and the decrease in *β*-sheets are believed to be due to the unfolding of the HSA in the presence of DA because of weak
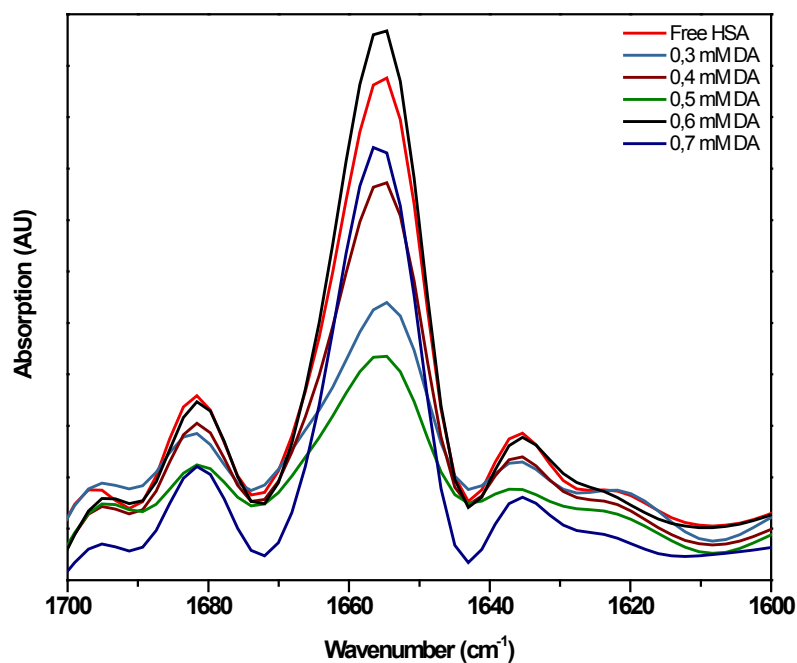
Figure 10. Deconvolution curve for determination the percentages for secondary structure of HSA in amide I.

Table 2. Secondary structure determination for amide I, amide II, and amide III regions for HSA free and HSA-DA complexes.

Bands	Range (cm^{-1})	Intensity %	Intensity %	Intensity %	Intensity %	Intensity %	Intensity %
		Free HSA	0.3 mM	0.4 mM	0.5 mM	0.6 mM	0.7 mM
Amide I			1700 - 1600 (cm^{-1})				
β-sheets	1614 - 1628	3	5	3	3	1	1
Random	1628 - 1643	12	11	11	9	11	11
α-helix	1645 - 1672	65	56	65	55	68	70
Turns	1674 - 1687	13	14	13	16	12	11
β-sheets (Anti)	1689 - 1700	7	14	8	17	8	7
Amide II			1600 - 1480 (cm^{-1})				
β-sheets	1484 - 1500	7	6	5	6	6	6
Random	1502 - 1531	25	19	17	13	18	19
α-helix	1533- 1564	22	20	32	26	32	34
Turns	1564 - 1585	19	20	18	18	18	18
β-sheets anti	1585 - 1600	27	35	28	37	26	23
Amide III			1320 - 1220 (cm^{-1})				
β-sheets	1222 - 1255	47	36	36	30	39	30
Random	1257 - 1281	18	18	19	19	20	20
Turns	1281 - 1302	15	20	23	28	20	29
α-helix	1302 - 1317	20	26	22	23	21	21

intermolecular forces between HSA and DA at C=O and C—N—H groups. This intermolecular interaction which is mainly due to collisions and weak interactions due to electrostatic forces between the HSA and DA causing unfolding of HSA to increase thus increasing the α-helix percentage. [15] [16] [34] [35]. It seems that the electrostatic forces between HSA and DA increase bonding in α-helix which is accompanied by decrease in β-sheets due to destabilization effects due to fast dynamic equilibrium which is consistent with the small binding constant value obtained from fluorescence in addition to weak hydrophobic contacts.

5. Discussion/Conclusions

In conclusion, the complexation of HSA-DA has been investigated using UV absorption spectroscopy, fluorescence spectroscopy, and FT-IR under physiological conditions. DA binds to HSA with binding constant of 4.4×10^2 and quenching constant of 1.32×10^9 L·mol^{-1}·s^{-1} at 25˚C.

The UV investigation repeatedly showed no complexation and a value for the binding constant was not determined due to the very weak interaction between DA and HSA when compared to added absorbance signals of individual absorbing HSA and DA. Fluorescence investigations indicate that the original fluorescence of HSA was quenched by DA through dynamic quenching mechanism which is consistent with the obtained value of quenching constants. Simply, DA must diffuse to HSA during the lifetime of the excited state. Once diffused and upon contact, Trp214 returns to its ground state. The small binding constant is in agreement with the quenching constant value.

There are several ways to distinguish between dynamic and static quenching. The first is to realize that upon complexation the newly formed complex usually has a different absorption spectrum from either of the complex components, therefore, changes on the absorption spectra are almost a diagnostic of a static quenching mechanism. The second hint usually is evident from the shape of the absorption spectra. Linear Stern-Volmer is almost always due to static quenching while non-linear is almost definitive criteria for either dynamic quenching due to purely collisional frequency or due to a mix of both static and dynamic quenching. Although dynamic and static processes are concurrently present in many systems, it is very important to realize the distinctive feature of the absorption spectra of such systems which result in an upward curvature which is not the case in HSA-DA system. Similar behavior in shape of the absorption spectra might be obtained in cases where there is more than one fluorophore accessible to the quencher *i.e.*, DA. In such cases, DA quenched Trp214 fluorophores on the surface but was not able to penetrate the hydrophobic interior of HSA due to hydrophobic forces from within the bulky HSA or the presence of charged quenchers such as the chloride ion of the dopamine hydrochloride and as a result DA would have limited surface intermolecular interaction due to inaccessibility of the interior Trp214 residue sites and only those residues on the

surface of the protein would be quenched. This is consistent with our findings in terms of fraction accessible for quenching of 5%. This behavior has been observed in protein fluorophore quenching by polar or charged quenchers. As a result, Stern-Volmer plots deviate from linearity toward the *x*-axis.

FT-IR spectra indicate increase in partial unfolding of the protein upon DA binding due to weak intermolecular hydrophobic electrostatic forces. The FT-IR results are consistent with fluorescence investigation.

The results reported in this paper are helpful to improve the understanding of the HSA interaction with DA. The biological significance of this investigation lies in the well-recognized role of HSA as a drug transporter to target specified organs in such a way that the target organ could be cured therefore it is very important to understand the various types of molecular interactions of HSA with drugs are essential in the drug delivery and in promotion alternative foundations for new pathways of drug delivery. DA is delivered using L-3,4-dihydroxyphenylalanine (L-DOPA), which is the precursor of DA, in treatment of Parkinson's disease due to lack of dopamine. We look forward to developing alternative ways to deliver DA more effectively instead of converting the precursor to dopamine. Now that we have such results indicating the quenched nature for fluorescence quenching, this could be the beginning to develop alternatives ways for enhancing the HSA-DA interactions enhancement to be able to deliver DA directly. Possible ways to achieve this goal could be by either derivatization of DA or by using nanoparticles functionalization.

Acknowledgements

Conflicts of Interest

The authors declare no conflicts of interest regarding the publication of this paper.

References

[1] Dewick, P.M. (2006) Chapter 11 Essentials of Organic Chemistry: For Students of Pharmacy, Medicinal Chemistry and Biological Chemistry. 1st Edition, Wiley, Hoboken.

[2] Arias-Carrión, *et al.* (2010) Dopaminergic Reward System: A Short Integrative Review. *International Archives of Medicine*, **3**, 24-29.
https://doi.org/10.1186/1755-7682-3-24

[3] Carlsson, A. (1959) The Occurrence, Distribution and Physiological Role of Catecholamines in the Nervous System. *Pharmacological Reviews*, **11**, 490-493.

[4] Narvaes, R. and Maria Martins de Almeida, R. (2014) Aggressive Behavior and Three Neurotransmitters: Dopamine, GABA, and Serotonin—A Review of the Last 10 Years. *Psychology & Neuroscience*, **7**, 601-607.
https://doi.org/10.3922/j.psns.2014.4.20

[5] Olguín, H.J., Guzmán, D.C., García, E.H. and Mejía, G.B. (2016) The Role of Dopa-

mine and Its Dysfunction as a Consequence of Oxidative Stress. *Oxidative Medicine and Cellular Longevity*, **2016**, Article ID 9730467.

[6]   Nobili, A. (2017) Dopamine Neuronal Loss Contributes to Memory and Reward Dysfunction in a Model of Alzheimer's Disease. *Nature Communications*, **8**, Article Number: 14727. https://doi.org/10.1038/ncomms14727

[7]   Kähkönen, S., Ahveninen, J., Pekkonen, E., Kaakkola, S., Huttunen, J., *et al.* (2002) Dopamine Modulates Involuntary Attention Shifting and Reorienting: An Electromagnetic Study. *Clinical Neurophysiology*, **113**, 1894-1902. https://doi.org/10.1016/S1388-2457(02)00305-X

[8]   Devos, D., Devedjian, J.-C. and Moreau, C. (2014) Is Dopamine Involved in Alzheimer's Disease? *Frontiers in Aging Neuroscince*, **6**, 1-6.

[9]   Devos, D., Devedjian, J.-C. and Moreau, C. (2017) Intracerebroventricular Dopamine for Parkinson's Disease. *Oncotarget*, **8**, 45034-45035. https://doi.org/10.18632/oncotarget.17596

[10] Triarhou, L.C. (2000-2013) Dopamine and Parkinson's Disease. Madame Curie Bioscience Database, Landes Bioscience.

[11] Alexander, G.E. (2004) Biology of Parkinson's Disease: Pathogenesis and Pathophysiology of a Multisystem Neurodegenerative Disorder. *Dialogues in Clinical Neurosciences*, **6**, 259-280.

[12] Blanco, G. and ocnalB, A. (2017) Medical Biochemistry. 1 Edition, Academic Press, Cambridge, Massachusetts.

[13] Alekseev, R.J. and Rebane, A.L. (2012) Protein Biochemistry, Synthesis, Structure and Cellular Functions. Nova Science Pub Inc., UK ed. Edition.

[14] He, X.M. and Carter, D.C. (1992) Atomic Structure and Chemistry of Human Serum Albumin. *Nature*, **358**, 209-215. https://doi.org/10.1038/358209a0

[15] Fasano, M., Curry, S., Terreno, E., Galliano, M., Fanali, G., Narciso, P., Notari, S. and Ascenzi, P. (2005) The Extraordinary Ligand Binding Properties of Human Serum Albumin. *IUBMB Life*, **57**, 787-796. https://doi.org/10.1080/15216540500404093

[16] Yang, F., Zhang, Y. and Liang, H. (2014) Interactive Association of Drugs Binding to Human Serum Albumin. *International Journal of Molecular Sciences*, **15**, 3580-3595. https://doi.org/10.3390/ijms15033580

[17] Roy, S. (2016) Review on Interaction of Serum Albumin with Drug Molecules. *Research and Reviews: Journal of Pharmacology and Toxicological Studies*, **4**, 7-16.

[18] Larsen, *et al.* (2016) Albumin-Based Drug Delivery: Harnessing Nature to Cure Disease. *Molecular and Cellular Therapies*, **4**, 3-14. https://doi.org/10.1186/s40591-016-0048-8

[19] Yasseen, Z.J. and Ghossain, M.E. (2016) Studies on Binding of Widely Used Drugs with Human Serum Albumin at Different Temperatures and PHs. *iMedPub Journals*, **5**, 3.

[20] Korolev, I.O. (2014) Alzheimer's Disease: A Clinical and Basic Science Review. *Medical Student Research Journal*, **4**, 24-33.

[21] An, *et al.* (2008) Main Hypotheses, Concepts and Theories in the Study of Alzheimer's Disease. *Life Science Journal*, **5**, 1-5.

[22] Karch, C.M., Cruchaga, C. and Goate, A.M. (2014) Alzheimer's Disease Genetics: From the Bench to the Clinic. *Neuron*, **83**, 11-26. https://doi.org/10.1016/j.neuron.2014.05.041

[23] Lloyd, A., Demetrius, L.A., Magistretti, P.J. and Pellerin, L. (2015) Alzheimer's Disease: The Amyloid Hypothesis and the Inverse Warburg Effect. *Frontiers in Physiology*, **5**, 1-25.

[24] Rasheed, N. and Alghasham, A. (2012) Central Dopaminergic System and Its Implications in Stress-Mediated Neurological Disorders and Gastric Ulcers: Short Review. *Advances in Pharmacological Sciences*, **2012**, Article ID: 182671.

[25] Beitz, J.M. (2014) Parkinson's Disease: A Review. *Frontiers in Bioscience*, **6**, 65-74. https://doi.org/10.2741/S415

[26] Jankovic, J. (2008) Parkinson's Disease: Clinical Features and Diagnosis. *Journal of Neurology, Neurosurgery, and Psychiatry*, **79**, 368-376. https://doi.org/10.1136/jnnp.2007.131045

[27] Hoang, Q.Q. (2014) Pathway for Parkinson Disease. *PNAS*, **111**, 2402-2403. https://doi.org/10.1073/pnas.1324284111

[28] Burns, J.M., Galvin, J.E., Roe, C.M., Morris, J.C. and McKeel, D.W. (2005) The Pathology of the Substantia Nigra in Alzheimer Disease with Extrapyramidal Signs. *Neurology*, **64**, 1397-1403. https://doi.org/10.1212/01.WNL.0000158423.05224.7F

[29] Storga, D., Vrecko, K., Birkmayer, J.G. and Reibnegger, G. (1996) Monoaminergic Neurotransmitters, Their Precursors and Metabolites in Brains of Alzheimer Patients. *Neuroscience Letters*, **203**, 29-32. https://doi.org/10.1016/0304-3940(95)12256-7

[30] Selkoe, D.J. and Hardy, J. (2016) The Amyloid Hypothesis of Alzheimer's Disease at 25 Years. *EMBO Molecular Medicine*, **8**, 595-608. https://doi.org/10.15252/emmm.201606210

[31] Karran, E. and Hardy, J. (2014) Antiamyloid Therapy for Alzheimer's Disease—Are We on the Right Road? *The New England Journal of Medicine*, **370**, 377-378. https://doi.org/10.1056/NEJMe1313943

[32] Stansley, B.J. and Yamamoto, B.K. (2015) L-Dopa and Brain Serotonin System Dysfunction. *Toxics*, **3**, 75-88. https://doi.org/10.3390/toxics3010075

[33] Quinlan, G.J., Greg, S., Martin, G.S. and Evans, T.W. (2005) Albumin: Biochemical Properties and Therapeutic Potential. *Hepatology*, **41**, 1211-1219. https://doi.org/10.1002/hep.20720

[34] Zsila, F., Bikadi, Z., Malik, D., Hari, P., Pechan, I., Berces, A. and Hazai, E. (2011) Evaluation of Drug-Human Serum Albumin Binding Interactions with Support Vector Machine Aided Online Automated Docking. *Structural Bioinformatics*, **27**, 1806-1813.

[35] Lee, P. and Wu, X. (2015) Review: Modifications of Human Serum Albumin and Their Binding Effect. *Current Pharmaceutical Design*, **21**, 1862-1865. https://doi.org/10.2174/1381612821666150302115025

[36] Segura-Aguilar, J., *et al.* (2014) Protective and Toxic Roles of Dopamine in Parkinson's Disease. *Journal of Neurochemistry*, **129**, 898-915. https://doi.org/10.1111/jnc.12686

[37] Darwish, S.M., Aiaidah, S.Y., Khalid, I.M., Abuteir, M.M. and Qawasmi, L. (2015) Spectroscopic Investigations of β-Amyloid Interactions with Propofol and L-Arginine. *Open Journal of Biophysics*, **5**, 50-67. https://doi.org/10.4236/ojbiphy.2015.52005

[38] Darwish, S.M., Abu sharkh, S.E., Abuteir, M.M., Makharza, S.A. and Abu-hadid, M.M. (2010) Spectroscopic Investigations of Pentobarbital Interaction with Human Serum Albumin. *Journal of Molecular Structure*, **963**, 122-129. https://doi.org/10.1016/j.molstruc.2009.10.023

[39] Zheng, X., Li, Z., Podariu, M.I. and Hage, D.S. (2014) Determination of Rate Constants and Equilibrium Constants for Solution-Phase Drug-Protein Interactions by Ultrafast Affinity Extraction. *Analytical Chemistry*, **86**, 6454-6460. https://doi.org/10.1021/ac501031y

[40] Lakowicz, J.R. (1990) Principles of Fluorescence Spectroscopy. Kluwer Academic Publishers/Plenum Press, Dordrecht/New York, Chapter 8.

[41] Chen, G.Z., Huang, X.Z., Xu, J.G., Zheng, Z.Z. and Wang, Z.B. (1990) Method of Fluorescence Analysis. Science Press, Chapter 4.

[42] Topală, T., Bodoki, A., Oprean, L. and Radu, O. (2014) Experimental Techniques Employed in the Study of Metals Complexes-DNA Interactions. *Farmacia*, **62**, 1049-1061.

[43] Ivanov, A.I., Zhbankov, R.G., Korolenko, E.A., *et al.* (1994) Infrared and Raman Spectroscopic Studies of the Structure of Human Serum Albumin under Various Ligand Loads. *Journal of Applied Spectroscopy*, **60**, 305.

[44] Wu, Y., Czarnik-Matusewicz, B., Murayama, K. and Ozaki, Y. (2000) Two-Dimensional Near-Infrared Spectroscopy Study of Human Serum Albumin in Aqueous Solutions: Using Overtones and Combination Modes to Monitor Temperature-Dependent Changes in the Secondary Structure. *The Journal of Physical Chemistry B*, **104**, 5840-5847. https://doi.org/10.1021/jp000537z

[45] Dukor, R.K., Chalmers, J.M. and Griffiths, P.R. (2001) Vibrational Spectroscopy in the Detection of Cancer. In: *Handbook of Vibrational Spectroscopy*, Wiley, Hoboken, Vol. 5, Chapter 3.

[46] Krimm, S. and Bandekar, J. (1986) Vibrational Spectroscopy and Conformation of Peptides, Polypeptides, and Proteins. *Advances in Protein Chemistry*, **38**, 181-364. https://doi.org/10.1016/S0065-3233(08)60528-8

[47] Ahmed-Ouameur, A., Diamantoglou, S., Sedaghat-Herati, M.R., Nafisi, Sh., Carpentier, R. and Tajmir-Riahi, H.A. (2006) The Effects of Drug Complexation on the Stability and Conformation of Human Serum Albumin. *Cell Biochemistry and Biophysics*, **45**, 203-213. https://doi.org/10.1385/CBB:45:2:203

[48] Lee, P. and Wu, X. (2002) Interaction of Drugs with Bovine and Human Serum Albumin. *Journal of Molecular Structure*, **614**, 227-232. https://doi.org/10.1016/S0022-2860(02)00256-9

[49] Polavarapu, P.L. (1998) Vibrational Spectra: Principles and Applications with Emphasis on Optical Activity. Elsevier Science, Amsterdam, Vol. 85, Chapter 14.

[50] Garidel, P. and Schott, H. (2006) Fourier-Transform Midinfrared Spectroscopy for Analysis and Screening of Liquid Protein Formulations: Part 1, Understanding Infrared Spectroscopy of Proteins. *BioProcess International*, **4**, 40-46.

[51] Garidel, P. and Schott, H. (2006) Fourier-Transform Midinfrared Spectroscopy for Analysis and Screening of Liquid Protein Formulations Part 2: Detailed Analysis and Applications. *BioProcess International*, **4**, 48-55.

[52] Huang, X., Guo, X.-F., Wang, H. and Zhang, H.-S. (2014) Analysis of Catecholamines and Related Compounds in One Whole Metabolic Pathway with High Performance Liquid Chromatography Based on Derivatization. *Arabian Journal of Chemistry*. https://doi.org/10.1016/j.arabjc.2014.11.038